Journal of Hydrology 622 (2023) 129727

Contents lists available at ScienceDirect

Journal of Hydrology

journal homepage: www.elsevier.com/locate/jhydrol

Research papers

Validation of Synthetic Design Hydrographs through 2D hydrodynamic modelling

Francesca Aureli [a,*], Federico Prost [a], Paolo Mignosa [a], Massimo Tomirotti [b]

[a] Department of Engineering and Architecture, University of Parma, Parco Area delle Scienze 181/A, 43124 Parma, Italy
[b] Department of Civil, Environmental, Architectural Engineering and Mathematics, University of Brescia, Via Branze 43, 25123 Brescia, Italy

ARTICLE INFO

This manuscript was handled by Corrado Corradini, Editor-in-Chief, with the assistance of Gokmen Tayfur, Associate Editor

Keywords:
River flood management
Synthetic Design Hydrographs (SDHs)
Historical flood hydrographs
2D hydraulic modelling

ABSTRACT

The procedure for the determination of Synthetic Design Hydrographs (SDHs), proposed in previous works, is validated by comparing the peak discharges obtained by routing a long series of historical floods and the synthetic floods at different stations along a complex river system.

At this aim, the 60 km long terminal stretch of the Dora Baltea river (Northern Italy) has been modelled according to fully 2D high resolution hydrodynamic approach. The fluvial branch is of considerable complexity due to a strong contraction induced by the presence of a narrow Roman bridge, which, during the most important flood events, causes the reactivation of a paleochannel and the flooding of a part of the city of Ivrea. The hydraulic model has been calibrated on the basis of the main historical floods. Then, all the historical floods over a period of more than 80 years (1939–2020) and the SDHs derived by the same series have been routed. Historical and synthetic peak discharges at two downstream stations have been then compared in probability plots. The results show that the peak discharge distributions derived by routing the historical floods and the SDHs compare well. This suggests that SDHs construction procedure is reliable and has statistical significance.

1. Introduction

The design of many flood protection measures in rivers and the optimization of flood plain management in view of risk mitigation often requires not only the estimation of the peak discharge, but also the volume and shape of the flood hydrograph (i.e. the distribution of flood volume over time) (Serinaldi and Grimaldi, 2011; Mediero et al., 2010; Rosbjerg et al., 2013; Alfieri et al., 2016; Brunner et al., 2016).

Indeed, a flood hydrograph can significantly modify its shape along a river reach by the effects due to water volumes temporarily stored in the main channel and in the flood plains, by the waters sometime diverted from the main riverbed or by flooding in the nearby campaigns. The amount of modification depends on a combination of hydrological inputs (peak discharge, volume and shape of the flood hydrograph) and on the characteristics of the river reach itself (main channel section geometry, flood plains extension, bottom slope, roughness, etc.). Hence, flood hydrographs with the same peak discharge, but different volumes and shapes, modify along the same reach in different ways.

There is then an interest to investigate if a design flood is capable to reasonably catch these effects, possibly together with a statistical characterization of the event rarity (Yue et al., 2002; Brunner et al., 2018a,b). In the absence of direct historical observations of water stages and reliable stage-discharge relationships, the estimation of design floods is often accomplished starting from design storms through hydrological models describing the most important catchment processes, namely the space–time precipitation field, the antecedent soil moisture conditions, the hydrological losses and the rainfall-runoff transformation. Approaches that simulate in an integrated way the rainfall-runoff transformation at the watershed scale and the hydrodynamics on the main streams with fully 2D-SWE distributed models have garnered great interest in the recent literature (Buttinger-Kreuzhuber et al., 2022; Barbero et al., 2022; Schubert et al., 2022). The speedup obtainable thanks to the implementation on GPU allows to execute many simulations with acceptable calculation times (Aureli et al., 2020). Several uncertainties however arise in the attribution of the return period to the resulting flood which is, for sake of simplicity, often considered the same as the input rainfall (Chapman and Maxwell, 1996; Viglione et al., 2009) even if this assumption is not always valid (Vangelis et al., 2022). Alternatively, rainfall-runoff continuous simulations or Monte Carlo procedures with stochastically generated input rainfall

* Corresponding author.
E-mail address: francesca.aureli@unipr.it (F. Aureli).

https://doi.org/10.1016/j.jhydrol.2023.129727
Received 15 March 2023; Received in revised form 10 May 2023; Accepted 23 May 2023
Available online 30 May 2023

can be adopted to generate a long flood record to be analyzed through a probabilistic approach (Kottegoda et al., 2014). This procedure is not always feasible or convenient due to the inadequacy of the available data necessary to run or calibrate the model and is often time consuming if the simulation-based model is computationally intensive (Zhang, 2020).

When direct historical observations of water levels and stage-discharge relationships are available, bivariate or multivariate flood frequency analyses have been considered for the definition of synthetic design floods (Sackl and Bergmann, 1987; Bergmann and Sackl, 1989; Goel et al., 1998; Yue, 1999; Shiau et al., 2006; Requena et al., 2013; Fischer and Schumann, 2021). The problem has been faced more recently by means of copula functions (Salvadori and De Michele, 2004; Wang et al., 2009; Chen et al., 2012; Huang et al., 2018; Kao & Chang, 2012; Peng et al., 2017; Brunner et al., 2017). The possible different return period approaches and formulations in a multivariate framework have been discussed by many authors (Yue et al., 1999; Yue, 2000, 2001a,b; Yue and Rasmussen, 2002; Gräler et al., 2013; Zhou et al. 2021). Indeed, in a multivariate framework the definition of an event with a given return period is not unique and must be determined by the problem at hand (Salvadori et al., 2011). In general, more than one couple peak discharge-flood volume must be considered for each return period, even if in some cases of application it might be desirable to have just one design realization for a specified return period (Brunner et al., 2016). Moreover, the shape of the hydrograph (i.e. the volume distribution around the peak) must be assumed a-posteriori, based on reasonable hypotheses on the response characteristics of the river basin.

Synthetic Design Hydrographs (SDHs) procedures (Tomirotti and Mignosa, 2017) can represent a possible alternative to derive design floods, especially when a sufficiently long time-series of historical hydrographs is available, as sometime occurs in rivers of some importance. Derived from the behaviour of the Flow Duration Frequency (FDF) reduction curves and of the Peak-Duration (PD) curve, the SDHs can account, in a very compact way, for the variability of the shapes of the observed hydrographs and synthesize the main features of the historical floods in a unique hydrograph. It is also evident that, given the versatility and ease of application, the procedure will receive a further boost from the enhancement of regional estimation techniques of the few parameters involved in SDHs definition (Hosking and Wallis, 1997; Zhang et al., 2008; Maione et al., 2003; Wagener and Montanari, 2011). Specific questions related to the most appropriate regionalization method for transferring SDHs from gauged to ungauged catchments and to which catchment characteristics are most important for the prediction of SDHs in the absence of direct observations were recently subject of research (Westerberg et al., 2016; Brunner et al, 2018b; Ganora et al., 2022).

In the context previously outlined, it is fundamental that the statistical significance of SDHs is duly tested. If definitively validated, SDHs will constitute a very useful and easily applicable tool, capable of avoiding more burdensome and time consuming procedures. With the aim of verifying whether the adoption of the SDHs could allow synthesizing the results obtainable from the routing of a long historical series, also in rivers characterized by complex flow dynamics, a fully 2D high-resolution hydrodynamic model of an Italian watercourse was set up and a long series of historical floods and of the derived SDHs were routed. The results were then compared at some stations along the river, in order to evaluate the statistical significance of the SDHs. The procedure required a long preparatory work both concerning the hydrological analysis and from the hydraulic modelling point of view, also given the extension of the involved domain and the characteristics of the river system considered.

The paper is structured as follows. In Section 2, the study area is presented and the historical discharge hydrographs available are introduced, statistically analyzed and elaborated to obtain the SDHs. In the same section, the high resolution fully 2D hydrodynamic model adopted for routing of historical hydrographs and SDHs is described. In Section 3, the results of the simulation of the historical hydrographs and of the SDHs are compared in terms of frequency distributions through probability plots and performance metrics at two river stations of interest. Section 4 discusses the statistical significance of the routed SDHs peak discharges together with their advantages, drawbacks and uncertainties, while the last Section 5 draws the conclusions.

2. Materials and methods

2.1. Study area

The Dora Baltea River originates in the Valle d'Aosta region (Northern Italy) at the foot of Mont Blanc, the highest peak in Italy (about 4800 m a.s.L.). The river flows for about 100 km in a west-east direction and then bends to the southeast and continues for about 60 km within the Piedmont region, to end into the Po, the most important Italian river. Object of the present analysis is the 60 km long river reach between the historical gauging station of Tavagnasco (Station A hereinafter) and the confluence into the Po River (Fig. 1). Since the establishment of the European Flood Directive 2007/60 (European Council, 2007), this stretch of the river is counted among the Italian *Areas of Potential Significant Flood Risk (APSFR)*. In the considered stretch (Fig. 1b) the river crosses the city of Ivrea (24000 inhabitants), which is located inside a morainic amphitheatre just where a substrate bedrock emerges and causes a significant constriction of the riverbed (Fig. 1c). In case of medium–high flowing discharges, the narrowest river cross-section, where is located an ancient Roman bridge (Fig. 1d) (Catalogo generale dei Beni Culturali, 2014), acts as a hydraulic control section. On the occasion of the most severe flood events, the water levels upstream the constriction increase enough to activate a paleochannel on the right side, and a significant fraction of the discharge coming from upstream inundates part of the city centre. In almost two hundred and seventy years this dynamic has been documented at least four times (Laio and Revelli, 2003), the last of which, in the recent years 1993 and 2000, caused extensive flooding with considerable damage and highlighted the extreme sensitivity of that territory to flood events. Downstream the city of Ivrea, the paleochannel reconnects with the present Dora Baltea riverbed and the diverted discharges come back to the main course. From there on the river flows in a relatively flat area that, especially close to the confluence with the Po River, is characterized by the presence of a marked terrace edge (Fig. 1b). Although the characteristics of the territory in this stretch are such as to configure limited hazard of flooding for the neighbouring areas, some storage depots for solid and liquid radioactive waste inside the terrace and close to the riverbed make anyway this area at very high risk.

2.2. Hydrological analysis

2.2.1. Database of historical floods

A 82 years long historical series of floods recorded at the Tavagnasco gauging station (drainage area 3313 km^2), located 10 km upstream the town of Ivrea (Fig. 1b), was collected. From 2002 to today, a continuous time-series of half-hourly water levels is available, whereas the older flood events, dating back to 1939, come from preventive operations of selecting, scanning, examining, cleaning and integrating the data recorded on paper through water level gauges. Water stages were then converted into discharges through the official stage-discharge relationships (Laio and Revelli, 2003; ARPAP, 2022; Claps et al., 2020). The selected data include the most important flood events in terms of both peak discharges and volumes from 1939 to 2020. From the 85 selected events, the peak Q_0 and maximum averaged discharges Q_D:

$$Q_D = \max\left(\frac{1}{D}\int_{t-D}^{t} Q(\tau)d\tau\right) \quad (1)$$

for durations D from 3 h up to $D_f = 96$ h have been sampled, being D_f

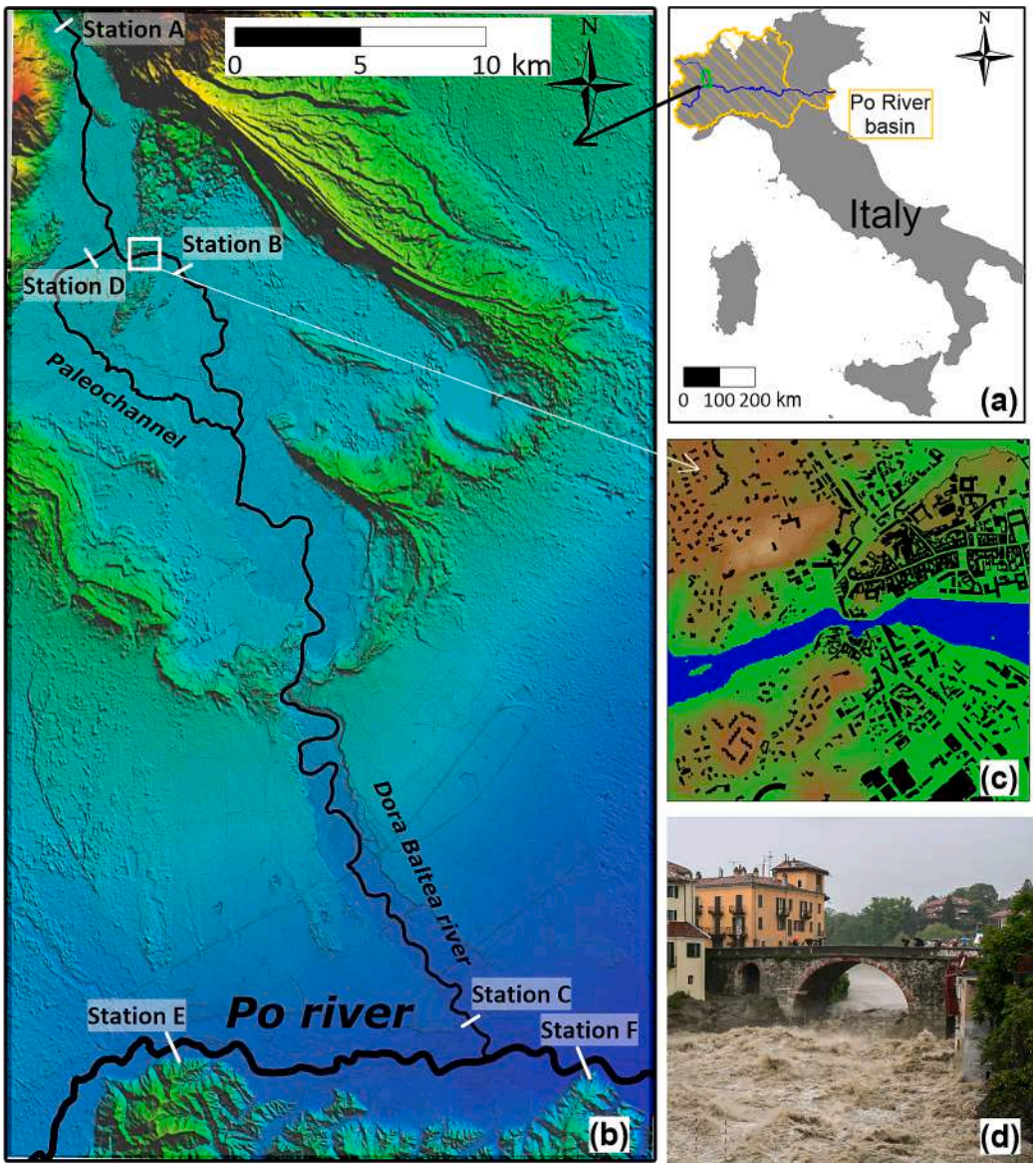

Fig. 1. a) Study site: Po river basin and Dora Baltea river in Italy; b) Study area: rivers system and river Stations of interest (A…F); c) Detail of Ivrea city centre and river constriction in the cross section of the Roman bridge; d) Roman bridge during a recent flood.

long enough to encompass the maximum historical total duration of flood events for the considered station. Together with each maximum average discharge, also the ratio r_D ($0 \leq r_D \leq 1$) between the time prior to the peak and the selected duration D has been extracted (Fig. 2). The resulting values are reported in Table 1 of the supplementary data.

2.2.2. Peak discharge probability distribution

Firstly, from the selected events the 82 AM peak discharge sample was extracted and tested for stationarity. MK (Mann, 1945; Kendall, 1975) and Pettitt (Pettitt, 1979) tests with significance level $\alpha = 0.05$ highlighted that, despite the length of the historical series, no gradual trends nor abrupt changes can be detected.

Hence, some probability distributions (Table 1), commonly adopted in the frequency analysis of extreme events, have been considered in order to derive the quantiles of the AM discharges $Q_0(T)$. Parameters estimation was based on the Method of *L-moments* (Hosking and Wallis, 1997). Plotting *L-skeweness* and *L-kurtosis* on the Hosking and Wallis *L-moment* ratio diagram (Fig. 3a) suggests that the best candidate models are the GEV and GLO distributions. Fig. 3b shows, on Gumbel probability chart, the data sample together with these two distributions. Both Akaike (AIC_c) and Bayesian (BIC) Information criteria (Akaike, 1973; Schwartz, 1978) confirm that the GLO distribution is preferable (minimum AIC_c and BIC) and GEV and Log Pearson III acceptable (ΔAIC_c and ΔBIC less than 2 with respect to GLO, Table 1) (Burnham & Anderson, 2002; Fabozzi et al., 2014). The GLO distribution was also recommended for use with UK flood data in the Flood Estimation Handbook (Institute of Hydrology, 1999). Even if a definitive judgment has not been expressed regarding the criterion that should actually be adopted in practical applications, especially in the case of small sample size or highly asymmetric distributions (Laio et al., 2009), the concordance of the two criteria and the relatively large sample size ($n = 82$) suggest that the GLO probability distribution is preferable and therefore the peak discharge quantiles $Q_0(T)$ were evaluated according to the expression:

$$Q(P) = \xi + \frac{\alpha}{k}\left[1 - \left(\frac{1-P}{P}\right)^k\right] \qquad k \neq 0 \tag{2}$$

with ξ (location), α (scale) and k (shape) parameters equal to 665.3 m^3/s, 180.0 m^3/s and − 0.320, respectively.

Peak discharges above 2500 and 3000 m^3s^{-1} are respectively

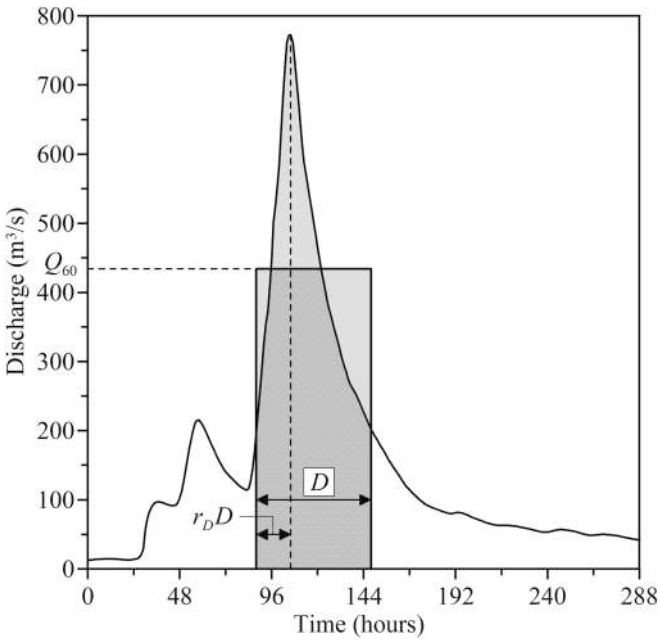

Fig. 2. Data sampling of Q_D and r_D from a historical hydrograph.

Table 1
Considered models, number of parameters, AICc and BIC difference with respect to the best model, Akaike weights based on AICc.

Model	N_{par}	ΔAIC_c	ΔBIC	w_i AIC_c
Gumbel	2	8.3	5.9	0.008
Log Normal 3 parameters (LN3)	3	6.2	6.2	0.022
Generalized Logistic (GLO)	3	0.0	0.0	0.486
Generalized Extreme Value (GEV)	3	1.3	1.3	0.252
Log Pearson III (LP3)	3	1.5	1.5	0.233

evaluated for return periods of 100 and 200 years, the standard for flood defence design in Italy. These high flow rates are such as to involve a very high hydraulic risk for the area under investigation as occurred, for example, for the flood events of the August 1993 and October 2000 which dramatically marked the Ivrea town and the surrounding areas.

2.3. Derivation of Synthetic Design Hydrographs

The procedure for the determination of SDHs (Tomirotti and Mignosa, 2017) is based on the estimation of the Flow Duration Frequency (FDF) reduction curves and of the Peak-Duration (PD) curve. The estimation of the FDF can be obtained (NERC, 1975) relating the quantiles $Q_D(T)$ to $Q_0(T)$ by means of the reduction ratio $\varepsilon_D(T)$:

$$\varepsilon_D(T) = \frac{Q_D(T)}{Q_0(T)} \tag{3}$$

The reduction ratio $\varepsilon_D(T)$ is in general a function of duration D and return period T, but in many practical cases it can be assumed independent of the latter. For a three-parameter distribution, like the GEV or the GLO, if the sample *L-CV* and *L-skewness* are constant with the duration D, ε_D becomes independent of T and reduces to the ratio of the averages of Q_D and Q_0:

$$\varepsilon_D = \frac{\mu(Q_D)}{\mu(Q_0)} \tag{4}$$

In the case here considered this condition is reasonably verified (Fig. 4), hence all the FDF curves can be deducted by a unique reduction ratio ε_D multiplied by the peak discharge quantiles $Q_0(T)$.

The expression of ε_D through a continuous and differentiable

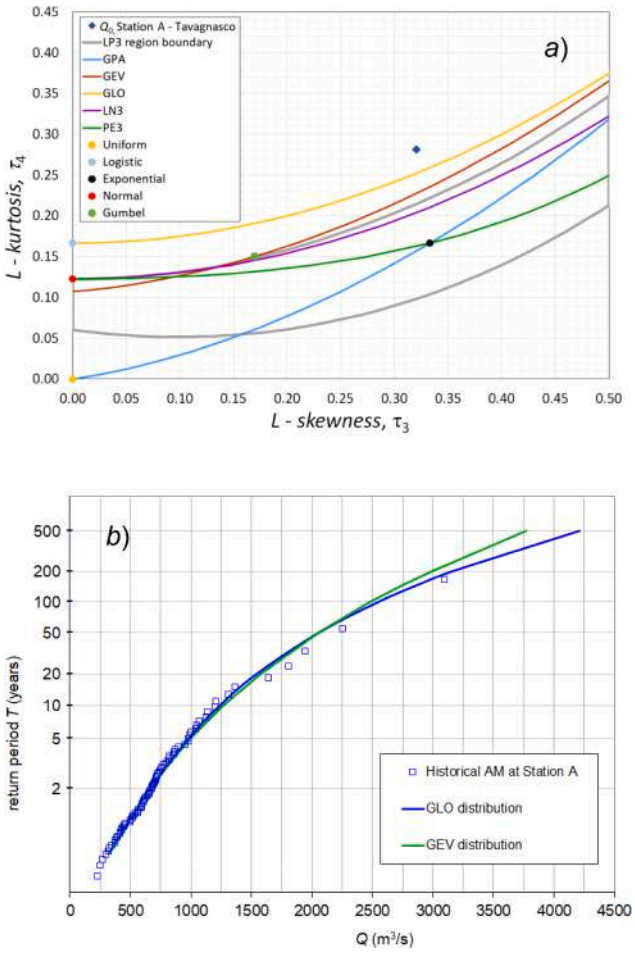

Fig. 3. a) *L-skeweness* (τ_3) and *L-kurtosis* (τ_4) ratio diagram; b) Q_0 data sample together with GEV and GLO probability distributions on a Gumbel chart.

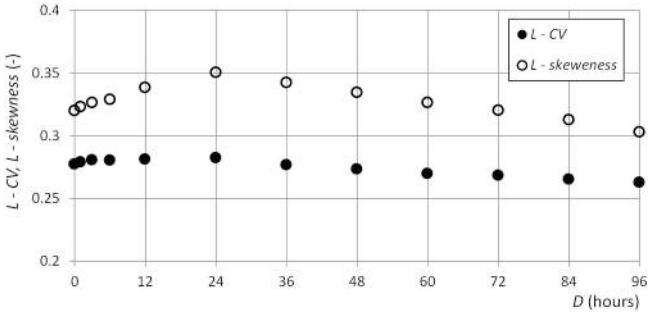

Fig. 4. *L-CV* and *L-skewness* as a function of the duration D.

function of D, even if not mandatory, can be advantageous for the subsequent derivation of SDHs. Based on the crossing properties of a given threshold value from continuous Gaussian stationary stochastic processes, Bacchi et al. (1992) derived the following formulation:

$$\varepsilon_D = \sqrt{\frac{\theta}{2D}\left[2 + e^{-\frac{4D}{\theta}} - \frac{3\theta}{4D}\left(1 - e^{-\frac{4D}{\theta}}\right)\right]} \tag{5}$$

Besides the advantages coming from its theoretical basis and from the presence of a unique parameter θ (dimensionally homogeneous with D), Equation (5) is particularly suitable to fit the empirical reduction ratios of large catchments. Moreover, Franchini and Galeati (2000) showed that θ can be correlated to the time of concentration of the catchment. For medium-size catchments (Ballarin et al., 2001), like the

one here considered, Equation (5) (here $\theta = 18.49$ h) does not always accurately fit the empirical reduction ratio (Fig. 5a). Following previous works (Aureli et al., 2021) it was therefore adopted the following more general form:

$$\varepsilon_D = \left[\frac{\theta}{2D}\left[2 + e^{-\frac{4D}{\theta}} - \frac{3\theta}{4D}\left(1 - e^{-\frac{4D}{\theta}}\right)\right]\right]^{\beta} \tag{6}$$

The higher flexibility given by the two parameters (θ and β) allows to better fit the sample values (here $\beta = 0.338$ and $\theta = 10.06$ h) (Fig. 5a). It is worth noting that other commonly adopted two-parameter functions, like that suggested by the UK National Environmental Research Council (NERC, 1975):

$$\varepsilon_D = (1 + bD)^{-c} \tag{7}$$

where b and c are positive parameters, could be used to fit empirical data as well (Ganora et al., 2022). Equation (7) is much more easy to manage but it has no inflection points and provides $d\varepsilon_D/dD|_{D=0} = -cb \neq 0$, contrary to Equations (5) and (6) for which $\lim_{D\to 0} d\varepsilon_D/dD = 0$. Hence, Equation (7) causes the SDHs to have a discontinuous derivative at the peak location (see section 2.3.2), which is rather unrealistic.

To obtain the Peak-Duration (PD) curve, which gives the average position r_D of the peak discharge in each duration D, the sampled r_D values were averaged for each duration D and interpolated with a two parameters asymptotic expression:

$$r_D = r_\infty + (0.5 - r_\infty)e^{-D/\vartheta} \tag{8}$$

with $r_\infty = 0.297$ (-) and $\vartheta = 10.9$ (hours) (Fig. 5b).

2.3.1. SDHs for the Dora Baltea a Tavagnasco

Once the FDF and PD curves have been estimated, the SDHs follow immediately through analytical derivation (Tomirotti and Mignosa, 2017) by imposing that the maximum average discharge in each duration coincides with the one predicted by the reduction curve. The shape of the hydrographs is then determined by the PD ratio expression. The synthetic hydrograph is therefore defined by the two conditions:

$$\int_{-r_D D}^{0} Q(\tau;T)d\tau = r_D D Q_D(T) \;\; ; \;\; \int_{0}^{(1-r_D)D} Q(\tau;T)d\tau = (1 - r_D)DQ_D(T) \tag{9}$$

before and after the peak, respectively. The rising and falling limbs $Q(t, T)$ are obtained by differentiating Equations (9) with respect to duration D, once the expression $Q_D(T) = \varepsilon_D Q_0(T)$ is introduced:

$$Q(t,T) = Q_0(T)\frac{\frac{d}{dD}[r_D D\varepsilon_D]_{D=D(t)}}{\frac{d}{dD}[r_D D]_{D=D(t)}}, \quad t = -r_D D \quad \left(-r_{D_f}D_f \leqslant t \leqslant 0\right) \tag{10a}$$

$$Q(t,T) = Q_0(T)\frac{\frac{d}{dD}[(1 - r_D)D\varepsilon_D]_{D=D(t)}}{\frac{d}{dD}[(1 - r_D)D]_{D=D(t)}}, \quad t = (1 - r_D)D \quad \left[0 \leqslant t \leqslant (1 - r_{D_f})D_f\right] \tag{10b}$$

Fig. 6 shows the SDHs obtained through the proposed procedure. Even if, strictly, a T-year hydrograph does not exist and a frequency can only be ascribed to a particular aspect of a hydrograph (Brunner et al., 2016), the same return period of the peak discharge, ranging from 2 to 500 years, was attributed to the SDHs as a whole. The discharge hydrographs recorded at Tavagnasco gauging station (Station A) for the August 1993 and October 2000 flood events are superimposed to the SDHs in Fig. 6 where, to facilitate the comparison, the time of peak of the historical hydrographs is set coincident with that of the SDHs.

2.4. Hydrodynamic modelling

A fully 2D hydrodynamic modelling was carried out with the aim of verifying whether the routing of the SDHs in a complex river system can actually be statistically representative of the propagation of a long series of historical floods. The availability of recent surveys and terrain models allows for the faithful simulation of the actual flood dynamics for more recent events, whereas flood events of several decades ago cannot be reproduced with the utmost historical fidelity, due to the changes in the river and territorial protection structures occurred in the intervening years. However, this is not a problem as the comparison between the results of the routing of historical floods and SDHs necessarily requires the same river description and hydrodynamic model to draw conclusions on the statistical validity of the SDHs.

The simulations were performed using the PARFLOOD code (Vacondio et al., 2014; Vacondio et al., 2016; Vacondio et al., 2017), developed at Parma University. The numerical model is based on an explicit finite volume discretization of the fully 2D Shallow Water Equations (SWEs) (Toro, 2001), expressed using the well-balanced formulation proposed by Liang and Marche (2009). The model is second-order accurate in both time and space, thanks to the adoption of the second-order Runge-Kutta method and of a depth-positive MUSCL extrapolation; the fluxes are evaluated using the HLLC approximate Riemann solver (Toro, 2001). The model is compatible with both Cartesian grids and structured non-uniform grids (Block Uniform Quadtree, BUQ), as detailed in Vacondio et al. (2017). The adoption of an unevenly distributed spatial resolution is useful for reducing the number of computational cells in the domain, and consequently the computational burden, while ensuring high accuracy in the areas of greatest interest (e.g., rivers, channels, buildings, hydraulic structures, embankments, etc.). The code is developed in the CUDA (Compute Unified Device Architecture) environment, which enables parallel computing on NVIDIA™ Graphics Processing Units (GPUs), leading to a drastic reduction in

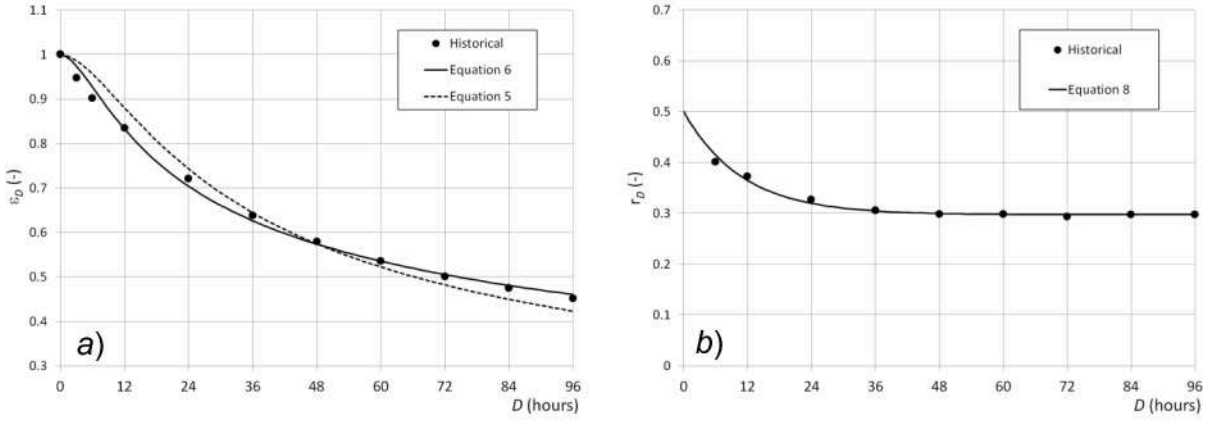

Fig. 5. a) Historical ε_D values and interpolating functions (Equations (5), (6)); b) Historical and interpolated peak position ratio (Equation (8)).

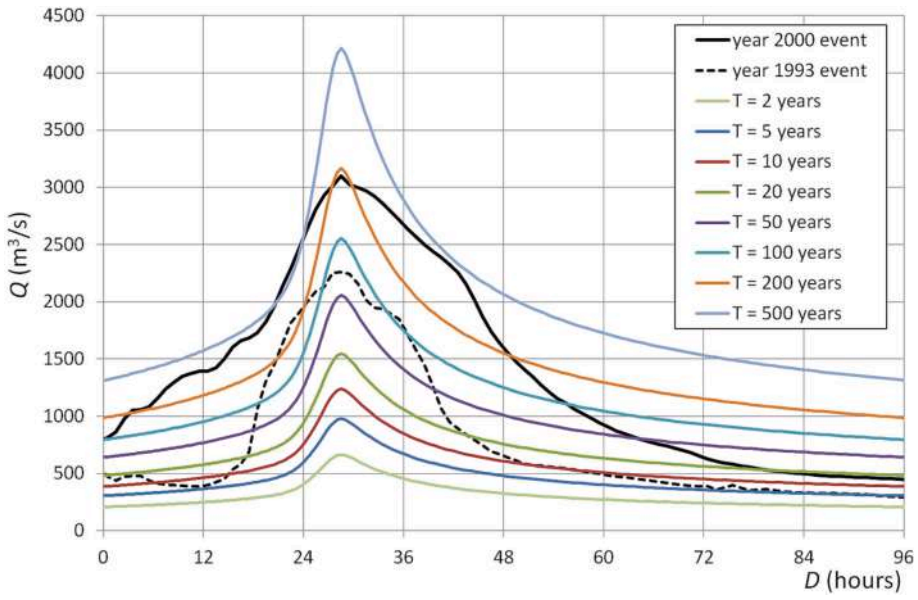

Fig. 6. SDHs for the Dora Baltea River at Tavagnasco gauging station (Station A) with the August 1993 and October 2000 flood hydrographs superimposed.

runtimes (of about two orders of magnitude) compared to serial codes, even for domains of several million cells (Vacondio et al., 2014). The good performances of the PARFLOOD model in both simulations of theoretical cases and practical applications over complex bathymetries are well documented in previous works to which the reader is referred for further details (Vacondio et al., 2016; Mignosa et al., 2018; Dazzi et al., 2019; Ferrari et al., 2020; Aureli et al., 2020; Dazzi et al., 2021). Among the approaches available for inclusion of bridges and other hydraulic structures in 2D numerical models, internal boundary conditions (IBC) were favoured in PARFLOOD thanks not only to their applicability to different flow conditions and structure types, but also to their suitability to predict the field-scale backwater effects induced by the fluid/structure interaction in case of high flows. The IBC implementation is described in detail by Dazzi et al. (2020a). An example of application of IBCs to bridges in urban flood modelling is reported in Dazzi et al. (2020b).

2.4.1. 2D discretization of the domain

A recent LiDAR survey provided a Digital Terrain Model (DTM) of the study area with 1 m × 1 m resolution, which was downsampled to 4 m × 4 m, considered adequate for this case. In the grid coarsening process, particular attention was paid to preserve the elevation of retaining structures along the streams and other thin linear topographic features in the domain (Sofia et al, 2014). A further pre-processing of the DTM was necessary to restore the embankment crest elevations that were not correctly described due to the removal of the bank vegetation cover from the raw LiDAR data, and to integrate in the DTM the bathymetric portion of the riverbed not detected due to the presence of water at the time of the survey. Ten bridges were introduced in the hydrodynamic model.

Starting from the DTM at 4 m × 4 m, a BUQ multiresolution grid with cells of variable size, from a minimum value of 4 m to the maximum of 16 m, was built. In order to model the flood propagation accurately, the main riverbed, the paleochannel and the urban areas were described with the highest resolution. Elsewhere, the spatial resolution was automatically relaxed by the pre-processing algorithm, as described in Vacondio et al. (2017). The calculation grid thus identified is made up of 4.3 million cells.

2.4.2. 2D Model calibration

The calibration of the model was carried out by simulating three important historical events (in order of importance 2000, 1993 and 1978), together with some recent flood events for which water levels at a downstream gauging station (Station C) were available. Historically, the first two flood events (Q_0 = 3100 and 2260 m^3/s at Station A, respectively) caused the diversion of part of the discharge into the paleochannel upstream of the Ivrea bottleneck, while the third (Q_0 = 1810 m^3/s at Station A) did not trigger it. On the basis of previous studies (Hydrodata, 2002), the computational domain was divided into active riverbeds (Manning $n = 0.037\ m^{1/3}s^{-1}$), floodplain areas ($n = 0.091\ m^{1/3}s^{-1}$) and floodable external areas ($n = 0.067\ m^{1/3}s^{-1}$).

It is worth noting that the triggering of the paleochannel is scarcely influenced by the bed roughness upstream the cross-section of the Roman bridge: since this section acts as a hydraulic control, the upstream levels, which are responsible for the entry into operation of the diversion, are essentially governed by the geometry of the narrower sections. This circumstance makes it difficult to calibrate the roughness in this area. Notwithstanding this, once the geometry is well described, the model has proved capable of correctly reproducing the three main historical flood events, with the triggering of the paleochannel only in the first two. Moreover, the simulation of two recent flood events (Fig. 7), even if not among the most severe ones (the first is generated by the superimposition of snowmelt and rainfall) confirms the satisfactorily reproduction of the observed and simulated water levels and timing in the gauged Station C, located almost at the end of the modelled reach.

2.4.3. Boundary and Initial Conditions

The series of selected historical floods and the derived SDHs were adopted as upstream boundary conditions (BC) at the inflow section of Tavagnasco (Station A, Fig. 1b). In the three years where comparable historical floods occurred, two events were considered in order to be sure to correctly reproduce the AM peak discharge series also at the intermediate (B) and downstream (C) stations of the river. For comparable events belonging to the same year, it could in fact take place the swap between maximum upstream and downstream peak discharge, the latter depending also on the shape and volume of the inflow hydrograph and not only on its peak discharge. Considering only the events with AM peak discharges at the inflow Station A could then lead to an incorrect evaluation of the sample of AM peak discharges at the intermediate and downstream stations assumed as reference for the results comparison.

As downstream BC, it was preferred to avoid the adoption of a not completely realistic one-to-one stage-discharge relationship at the end

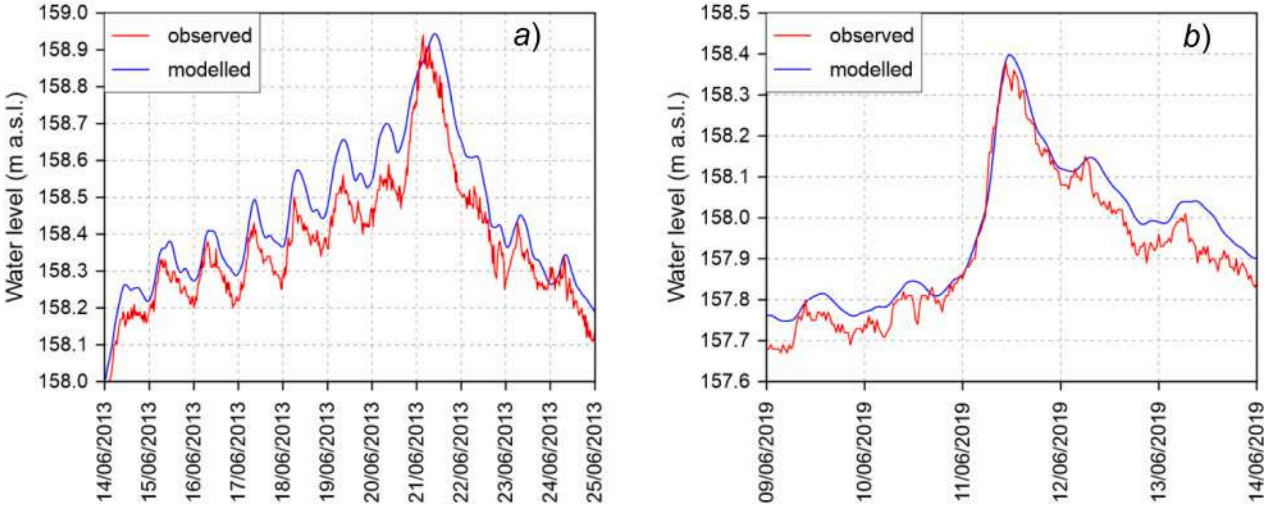

Fig. 7. Observed and modelled water levels at station C for the historical events of a) June 2013 and b) June 2019.

of the considered reach, where the flow is always subcritical and might be affected by backwater from the Po River. Instead, a sufficiently long stretch of this major river was also added to the model, imposing a stage-discharge relationship as downstream BC at Station F, and a constant medium–high discharge value as upstream BC at Station E (Fig. 1b). A sensitivity analysis carried on changing the value of the discharge at the upstream BC showed no influence on the hydrodynamic conditions even at the most downstream gauging station of interest on the Dora Baltea River (Station C).

Initial conditions were obtained through preliminary simulations in steady state conditions in correspondence of the initial value of each inflow discharge hydrographs considered.

3. Results

Fig. 8 shows for the August 1978 (Fig. 8a) and October 2000 (Fig. 8b) historical events: i) the inflow hydrograph at Station A; ii) the simulated discharge hydrograph in a river station between the diversion and the return of the waters in the main riverbed (Station B, see Fig. 1b for the location); iii) the simulated discharge hydrograph in a cross-section located almost at the end of the modelled river stretch (Station C). Fig. 8b shows also the diverted flood hydrograph at Station D along the paleochannel (see Fig. 1b for the location of Station D). The August 1978 flood event did not trigger the operation of the paleochannel, so the reduction of the peak discharge along the reach is exclusively due to the routing effect. The October 2000 event, on the contrary, caused the diversion of a significant portion of the flood into the paleochannel, so that the discharge and volume reduction at the intermediate Station B is due to the combined effect of routing and diversion. Most of the diverted waters then returns to the main riverbed upstream Station C, consequently there the peak discharge and the volume of the flood are decidedly higher than those at the intermediate Station B.

Fig. 9 shows the inflow (Station A) and routed SDHs (Stations B, C and D) at the same selected Stations. Recalling that each SDH has been assigned, till now in a somewhat arbitrary manner, a unique return period, no diversion occurs in the paleochannel up to $T = 20$ years, therefore a null discharge flows at Station D. From $T = 50$ years on, an increasing part of the volume of the synthetic flood is unable to pass through the narrow cross-section of the Roman bridge and the upstream levels rise enough to trigger the diversion into the paleochannel. For T = 500 years the peak discharges in the river and in the paleochannel are almost the same.

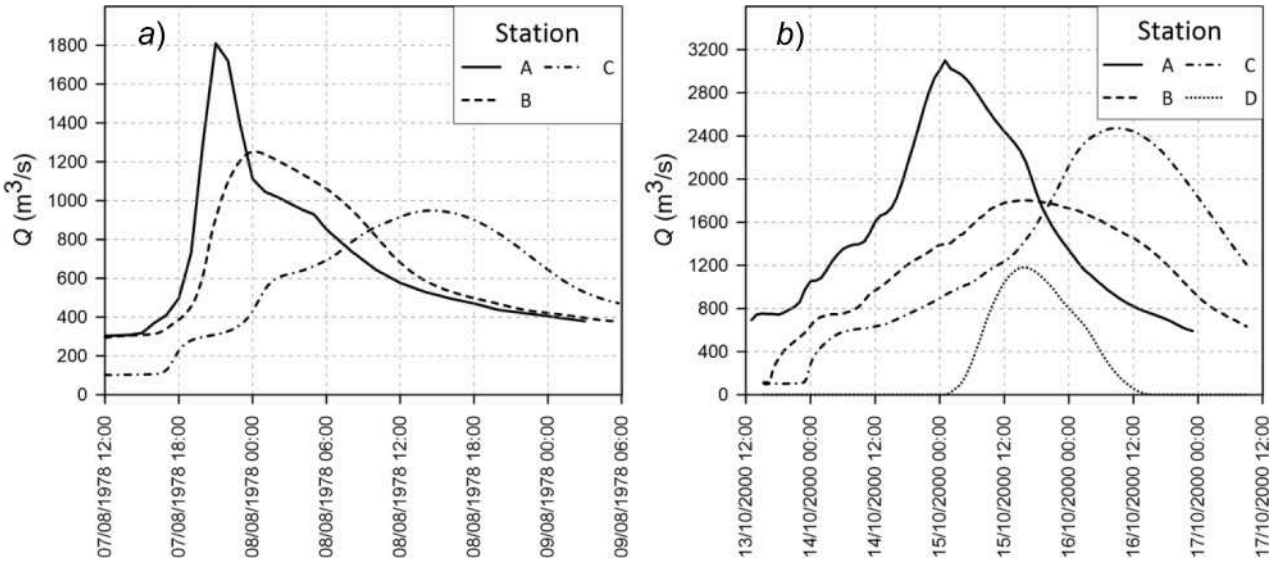

Fig. 8. Observed flood hydrographs at Station A and simulated flood hydrographs at Stations B (intermediate) and C (downstream) for a) the August 1978 and b) October 2000 historical events. For the August 2000 flood event the diverted flood hydrograph at Station D is also shown.

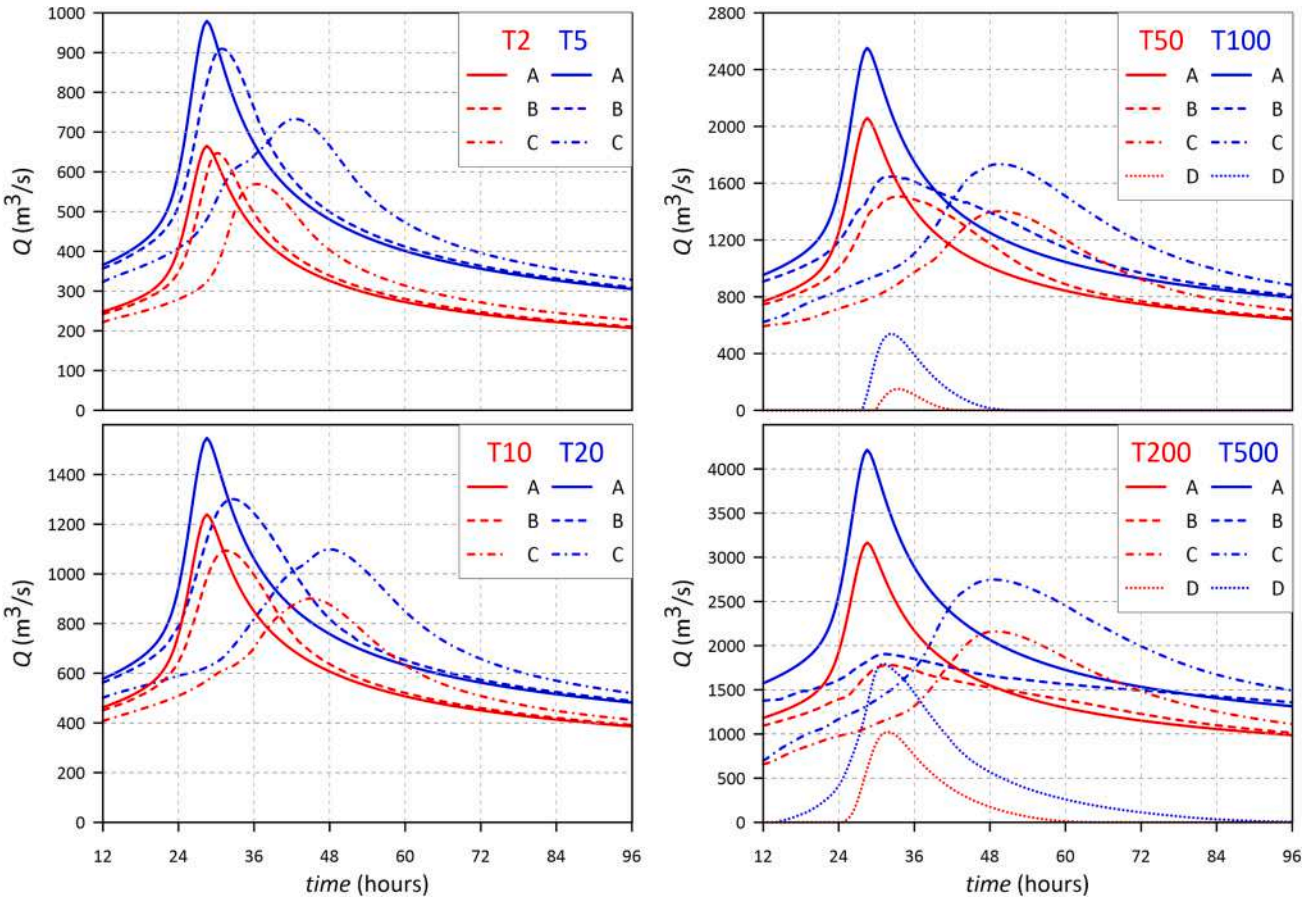

Fig. 9. Inflow (Station A) and routed SDHs at Stations B-C-D for return periods T equal to 2, 5, 10, 20, 50, 100, 200 and 500 years.

It is also worth noting that the peak flow attenuation in the river reach from Station A to Station C increases significantly with the return period T, spanning from 14% for $T = 2$ years to 35% for $T = 500$ years. This is a consequence of the temporary storage of flood volumes upstream of the Roman bridge constriction and in the wide floodplains in the middle stretch of the river, together with the different flood propagation times in the main riverbed and in the paleochannel.

Fig. 10 shows a detail of the flooded area and the maximum water depths (not simultaneous) close to the city of Ivrea for the simulation of the 200 years SDH. Upstream of the constriction, where the Roman bridge is located, maximum water depths reach 17 m and the water levels exceed the local ground levels which causes the triggering of the paleochannel. This is empirically consistent with what happened historically during the October 2000 flood event, despite some changes occurred to the morphology of the area, which however did not involve the modification of the invert level of the rocky sill beyond which the overflow toward the paleochannel begins.

Fig. 11a,b summarize the more significant results of the comparison between historical events and SDHs. In a Gumbel probability chart, Fig. 11a shows:

1. the frequency distribution of the sample of historical AM of peak inflow discharges at Station A (the same reported in Fig. 3b);
2. the probability distribution (GLO) fitted to 1) (the same reported in Fig. 3b);
3. the frequency distribution of the sample of simulated AM peak discharges derived by the routing of the historical events at the Station B downstream the diversion;
4. the probability distribution fitted to 3); the same model selection criteria (AIC_c and BIC) suggest in this case the choice of a Gumbel probability distribution, not a heavy tailed distribution like the GLO. This change is justified by the amount of the diverted waters, increasing with the return period of the event considered.
5. the peak discharges derived by the routing of the SDHs at Station B; as plotting position, the same return period attached to each inflow SDH was also attributed to the corresponding outflow peak discharge obtained after the routing.

Fig. 11b shows the same data 1), 2), whereas 3), 4) and 5) refer to Station C at the end of the simulated river reach. For this station, as for Station A, the selected probability distribution fitted to 3) was a GLO.

Table 2 shows the peak discharge quantiles ($T = 2…500$ years) obtained by the probability distribution fitted to the sample of the routed AM historical events ($Q_{distr.}$) and the peak discharges obtained by routing the SDHs (Q_{SDH}) at Stations B and C to which the same return period of each inflow SDH was attributed. The Percentage Error $PE(Q) = 100(Q_{dist.} - Q_{SDH})/Q_{dist.}$ maintains small also for high return periods in both Stations, without any evident trend. The same holds for the RMSE of Q

$$RMSE(Q) = \sqrt{\frac{1}{m}\sum \left(Q_{dist.}(T) - Q_{SDH}(T)\right)^2} \tag{11}$$

which assumes the values of 49 m^3/s and 43 m^3/s for Stations B and C, respectively ($m = 8$ is the number of selected return periods).

The results obtained at the intermediate Station B at the downstream Station C confirm that SDHs are capable to synthesize and reproduce the main characteristics of the historical flood events, also in complex river system such as the one here considered. This was not trivial, given the significant modification observed among the inflow (Station A), the outflow (Station C) and, above all, the intermediate (Station B) peak discharge values.

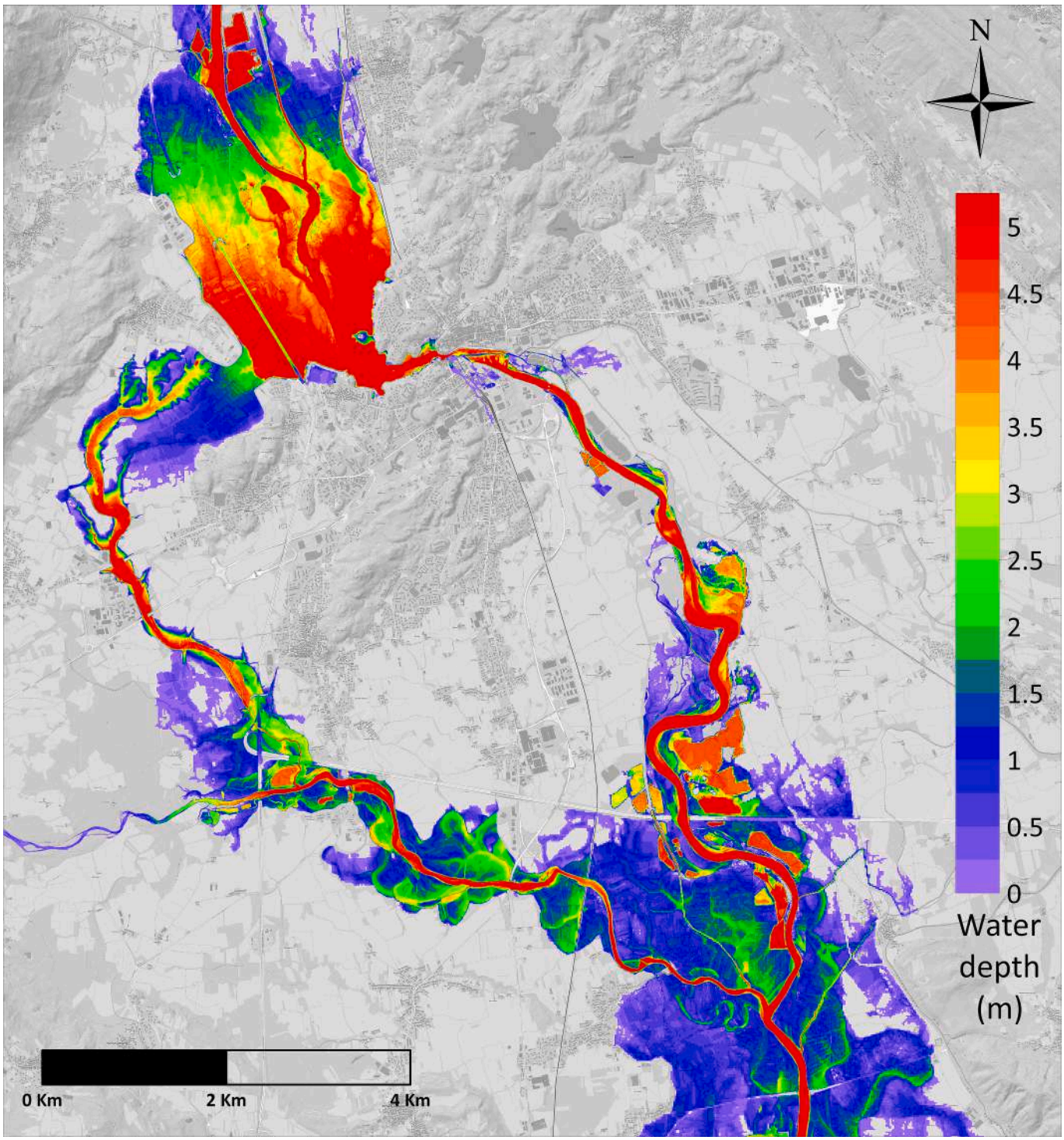

Fig. 10. Flooded area and maximum water depths (not simultaneous) close to the city of Ivrea for the simulation of the 200 years SDH (color map was saturated over 5 m).

4. Discussion

The proposed procedure has a twofold advantage. Firstly, even when a historical series of floods is available (and this is not always the case), it allows evaluating the distribution of peak discharges at a downstream section simply routing very few synthetic floods instead of a long series of historical ones. While this may not be a problem when 1D models are adequate to describe the routing effects along the river reach, this is very beneficial (if not even necessary) when a high-resolution 2D model is required, like in the case here considered of a complex river reach with constrictions, wide floodplains and even diversions into a paleochannel. The PARFLOOD model adopted in the present work boasts a very high computational efficiency, thanks to its implementation on GPUs, which, other conditions being equal, guarantees speedups of two orders of magnitude with respect to serial CPU codes. In the specific case, where the terrain model has been described with 4.3 million of cells, the smallest of which are 4 $\times$ 4 m, the ratio between physical and computational time is of the order of 11–25 on a GPU NVIDIA Ampere® A100,

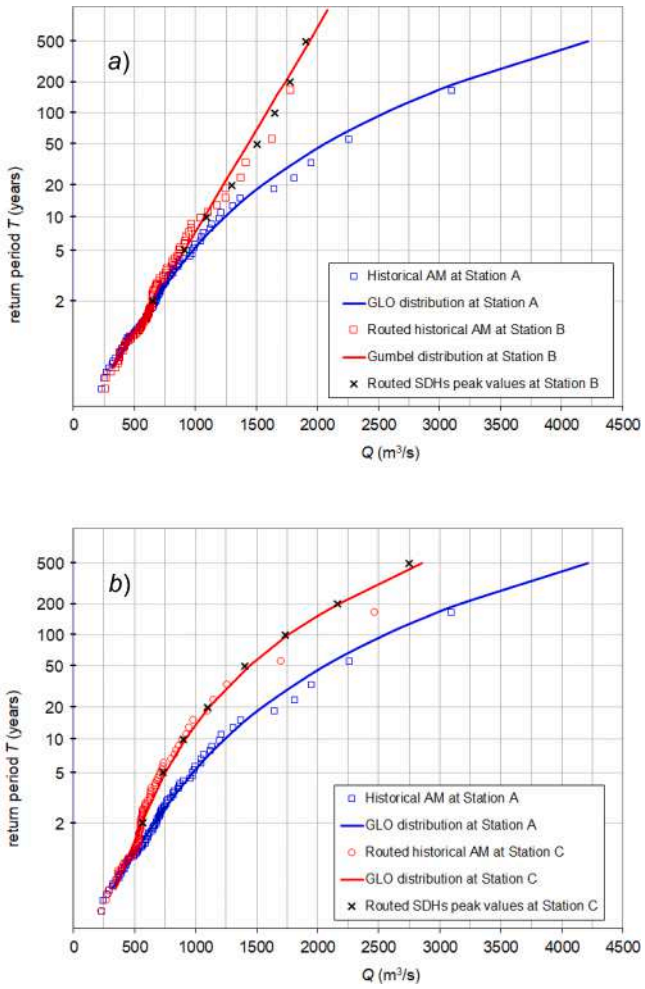

Fig. 11. AM frequency and probability distributions at a) the intermediate Station B and at b) the downstream Station C.

Table 2
Peak discharge quantiles $Q(T)$ (m^3/s) derived from GLO (Stations A and C) and Gumbel (Station B) distributions, routed SDHs peak values at Stations B and C and Percentage Errors.

	Station A	Station B			Station C		
T	$Q_{distr.}$	$Q_{distr.}$	Q_{SDH}	$PE(Q)$	$Q_{distr.}$	Q_{SDH}	$PE(Q)$
2	665	661	647	2.1	557	569	−2.2
5	980	908	909	−0.1	753	733	2.7
10	1239	1071	1094	−2.1	916	901	1.6
20	1547	1228	1301	−5.9	1112	1099	1.2
50	2059	1430	1507	−5.4	1441	1402	2.7
100	2553	1582	1649	−4.2	1761	1734	1.5
200	3167	1733	1777	−2.5	2163	2161	0.1
500	4216	1933	1904	1.5	2856	2747	3.8

depending on the event considered and the area actually flooded. This means that the simulation of a synthetic hydrograph lasting 96 h (physical time) requires a computational time of 4–10 h. The simulation of eight SDHs (from $T = 2$ to $T = 500$ years) requires a total computational time of about 60 h to be completed. By simulating only the most significant events for the design of defence works or for the definition of flood maps (50–500 years), as required for example by the EU flood directive 2007/60, then the calculation times can also be halved. The simulation of the entire historical series (85 events in the case here considered) instead requires an order of magnitude higher simulation time. The same holds if more than one bivariate design hyetograph for each return period or many Monte Carlo simulations have to be carried on. Of course, it is also possible to run the simulations in parallel, but it is not so common to have many GPUs of equal power available.

A further advantage of the SDHs is that they can be regionalized. In the present work we have used a river section with a very long historical series, which is quite rare in Italy but also in the rest of the world, in order to make the comparison more reliable for return periods comparable with those usually adopted in the river flood management (100–200 years in Italy). However, the procedure can also be applied to river sections where shorter time series are available or even in the absence of local records. In these cases the regionalization of SDHs requires three steps: 1) the estimation of the quantiles $Q_0(T)$, for which many different approaches are available in literature (Hosking & Wallis, 1997, Rosbjerg et al, 2013, Castellarin et al., 2012, De Michele and Rosso, 2001; De Michele and Rosso, 2002; Laio et al., 2011); 2) the estimate of the FDF reduction curves. If Equation (4) holds, this evaluation boils down to the estimate of the parameter/s (one or two, depending on the expression used) of the reduction coefficient ε_D which can in turn be based on the ratios between the averages of $\mu(Q_D)$ and $\mu(Q_0)$, for which even a relatively short period of observation can be adequate. In the total absence of observations, the parameters of the functional dependence of ε_D from D (Equations (5), 6, 7 or others) can be estimated using a set of watershed attributes derived from terrain analysis, land use features and climatic indexes through different regionalization methods (multiple linear regression techniques, canonical correlation analysis, spatial methods, methods based on the formation of homogeneous regions, among others) (Maione et al. 2003, Brunner et al., 2018b, Ganora et al., 2022); 3) the estimation of Peak-Duration (PD) curve through Equation (8) or other similar equations. Once again, in the total absence of local observations it is necessary to rely on regional estimates. This aspect has been little addressed in the literature, but it is worth noting that the definition of the synthetic hydrograph is not so sensitive to the choice of the PD curve, so that some authors (Ganora et al., 2022) assume a unique constant value of r_D for all D; the same approach is used for example in the derivation of the Chicago Design Storm (Keifer and Chu, 1957). Maione et al. (2003) addressed this problem for the regionalization of SDHs along the Po River (Northern Italy) by interpolation of the empirical patterns available at the gauging stations, after standardisation of the duration D by the local value of the temporal parameter θ of Equation (5). The writers have an advanced study in progress on this topic concerning many northern Italian rivers.

As all the models based on statistical analysis, the results obtained are inherently uncertain, and some assessment of the magnitude of uncertainty should be made in order to exploit the results with maximum confidence. As the main goal of the entire procedure is the estimation of the water levels of assigned exceedance probability along a river reach, the overall uncertainty depends on:

1) the estimation of the peak discharge quantiles at the upstream BC (inflow section). To this end, once verified the stationarity of the historical series, the longer the data set the better. In the specific case here considered, the data spans a period of 82 years, which is quite uncommon. However, since the design of river defences and the management of residual flood risk require considering rather rare events (T = 100–500 years), an estimate of the uncertainty of the estimated quantiles is necessary. For this purpose, confidence intervals (CIs) of estimated quantiles through 10^4 Monte Carlo simulations (Hosking & Wallis, 1997, Talbot, 2023) have been evaluated for a confidence level of 80% (Fig. 12). The CIs noticeably widen for $T = 100$ and especially for $T = 200$ and $T = 500$ years. Luckily, the relation between discharges and water levels in open sections is less than linear, so that differences in discharge are dampened in terms of water levels. It is worth noting, however, that a peak discharge of 6000 m^3/s, as indicated by the upper bound of the confidence curve for $T = 500$ years, could not even reach Station A due to a series of bottlenecks present in the upstream river reach which would give

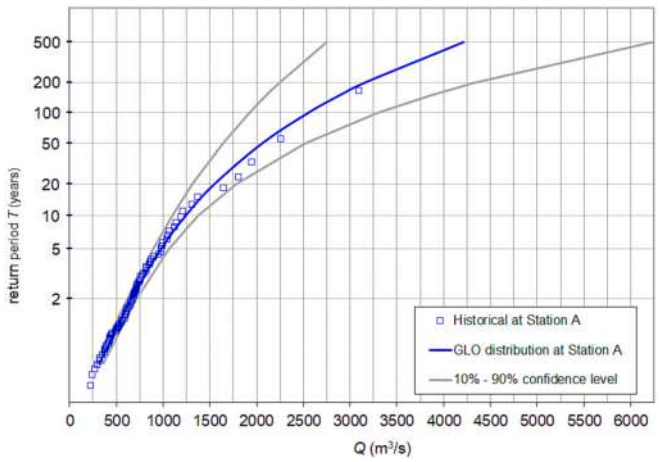

Fig. 12. Q_0 sample frequency distribution, fitted GLO probability distribution and 10% − 90% confidence level (Tavagnasco gauging station - Station A).

origin to extensive flooding and consequent peak discharge attenuation. In these situations, integrated hydrological-hydraulic models based on 2D-SWE equations can usefully complement purely statistical evaluations, narrowing the bandwidth of the confidence intervals, especially for high return periods.

2) the validity of Equation (4), which requires that the same parent distribution can be assumed for all the samples of Q_D and, if a three parameter distribution is selected, that *L-CV* and *L-skewness* are reasonably constant with the duration D. This last condition is not always verified, especially for small watersheds. In this latter case ε_D is no more independent from T and then FDF(T) reduction curves should be evaluated through the statistical analysis of the whole set of Q_D samples;
3) if Equation (4) holds, the estimation of the reduction coefficients and their fitting with a one- (Equation (5) or two- (Equations (6), 7) parameter equation. To evaluate a confidence interval of ε_D, a bootstrap technique (5000 random samples with replacements) was applied (Efron & Tibshirani, 1994). Fig. 13 shows the historical values of ε_D (the same reported in Fig. 5a) together with the 95% confidence intervals. For the duration D = 96 h the confidence interval spans in the quite narrow range 0.416–0.487, roughly ± 8% of the historical value (0.451).

As regards the uncertainty related to the interpolation of ε_D, it is worth noting that this is not a mandatory step, as SDH can be numerically evaluated using the estimated ε_D values directly (linearly interpolating between them). However, as previously recalled, interpolation with a one or two-parameters equation is necessary for regionalization purposes. As an example, Fig. 14a shows the comparison between the non-dimensional SDHs derived by fitting the two-parameter Equation (6) and the more parsimonious one-parameter Equation (5) to the ε_D values. Shape differences are appreciable not only in the tails, but also around the peak. The overall volumes of the SDHs are also significantly different (V(Eq.6)/V(Eq.5) = 1.089) since for the maximum duration D_f = 96 h the interpolated reduction coefficients are equal to 0.460 and 0.423 (Fig. 5a) adopting Equation (6) and Equation (5) respectively (whereas the historical value is 0.451).

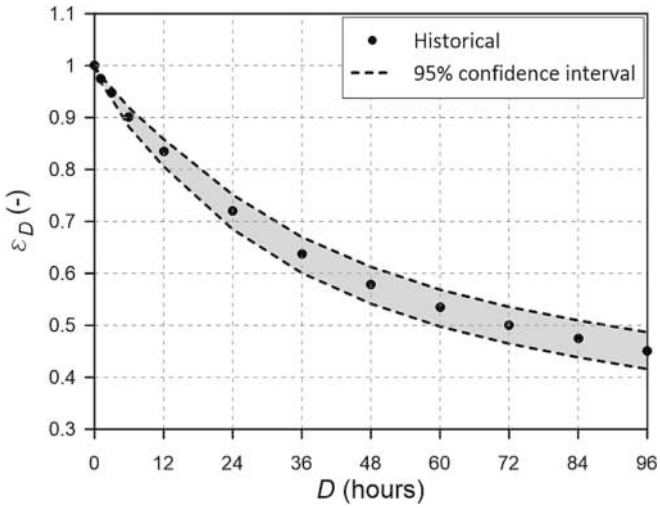

Fig. 13. Historical values of ε_D together with the 95% confidence interval.

Fig. 14b compares in a Q - Q plot the routed peak discharges at Stations B and C obtained imposing the two SDH shapes as upstream BC in the hydrodynamic model. Even if the overall volume of the hydrograph derived with Equation (5) is smaller, slightly increased values of Q_{peak} are obtained with this SDH at Station C. This is due to the greater volumes contained in the flood hydrograph around the peak, which causes less attenuation along the river reach and highlights the importance of defining not only the peak discharge and the overall volume of the hydrograph, but also the distribution of the volumes around the peak. The choice of the shape of the hydrograph, often considered secondary also in a bivariate framework, has actually proved to be fundamental in many other circumstances (Tomirotti and Mignosa, 2017).

To the aforementioned hydrological uncertainties must be added those inherent in:

4) the hydrodynamic model adopted. Fully 2D, shock capturing models are mandatory in complex river networks, as the one here considered, where flow transitions frequently occur. As an example, Fig. 15 shows the map of computed Froude numbers close to the Roman bridge at the passage of the peak flood during the October 2000 flood event. Transitions between sub- and supercritical flows and vice versa (hydraulic jumps) are recognizable. Simplified models (based on diffusive or local-inertial approximations equations), are not able to catch this behaviour at all (Costabile et al. 2020; Mignosa et al., 2018).
5) the adequate geometric description of the river and of the floodable areas. Since Lidar-based DTMs have become widespread and relatively cheap, numerous studies have been performed to analyze the sensitivity of hydrodynamic models with respect to spatial resolution (Cook and Merwade, 2009; Papaioannou et al., 2016; Jiang et al., 2022). In the case study here considered, the availability of a high resolution DTM integrated with terrestrial topographic data proved necessary to describe the narrower part of the river bed which controls the hydrodynamics close to the Roman bridge and the triggering of the paleochannel.
6) the evaluation (calibration) of the roughness. Depending on available data, different automatic procedures can be used for calibration (Aricò et al., 2009; Ferrari et al., 2022); in their absence, land use maps, literature and expert knowledge may guide in selecting the Manning parameters. In the present case, few level data were available just in the downstream section (Station C) and this prevents from an accurate and distributed calibration of roughness, since equifinality of model parameterisation can occur (Fabio et al., 2010). Having to simulate a long series of historical events, the roughness of the watercourse has certainly changed over time. Actually, river modifications concerned not only the roughness, but also the morphological changes occurred over almost a century, which are known only qualitatively on the basis of historical maps. The lack of knowledge of the geometry of the past and the absence of water level measurements (except at the historical station of Tavagnasco) therefore do not allow validating the correct reproduction of each historical event. However, this was not the aim of the work, which was instead that of comparing two hydrological boundary conditions

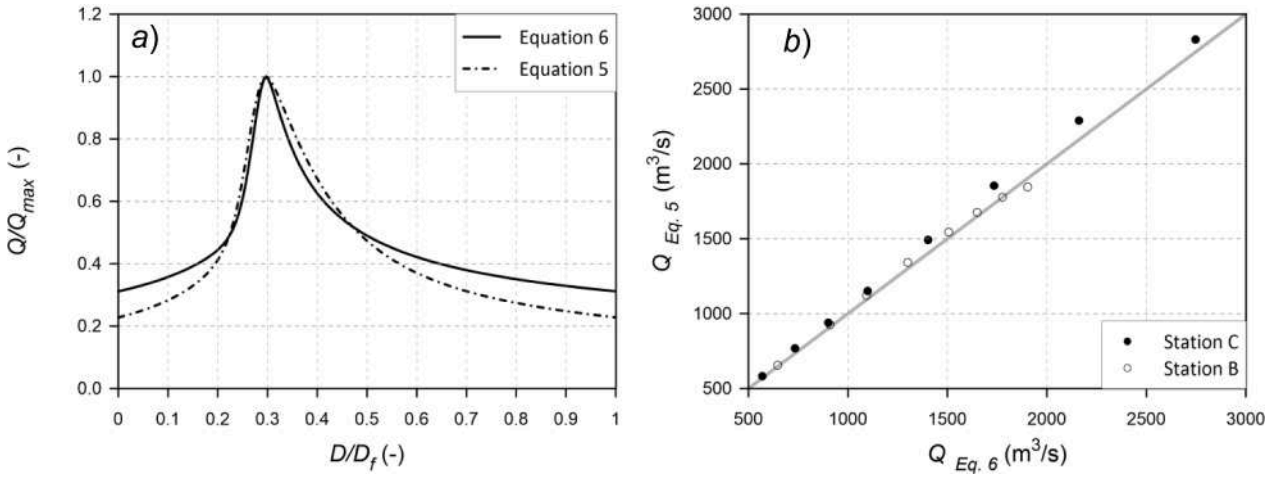

Fig. 14. a) Non dimensional SDHs obtained with Equation (5) and Equation (6) and b) routed peak discharges at Stations B and C with the two SDH shapes.

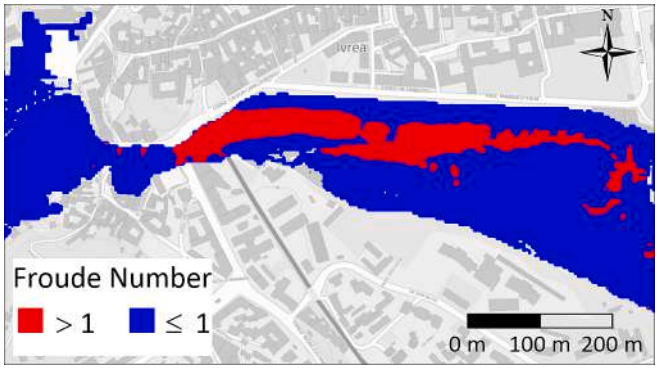

Fig. 15. Map of computed Froude numbers at the passage of the peak flood during October 2000 flood event close to the Roman bridge of Ivrea.

(a long historical series and few synthetic hydrographs) with other conditions being equal, i.e. as if all the events occurred in the same river configuration (the current one). By keeping the geometry (and roughness) of the watercourse constant and by varying only the boundary conditions, it is in fact possible to appreciate whether the synthetic hydrographs are capable of reproducing well the propagation phenomena that occur along the river. On the other hand, the same assumption is usually introduced in the hydrologic/hydraulic simulations aimed at the design of flood management measures.

It is worth noting, however, that the model uncertainties 4), 5) and 6) previously highlighted are also typical of all the other hydrological approaches too.

5. Conclusions

The procedure for the determination of Synthetic Design Hydrographs (SDHs), proposed in previous works, was validated by comparing the peak discharges at different stations along a complex river system, obtained by routing a long series of historical floods and the synthetic floods in a fully 2D hydrodynamic approach. The comparison confirms that the SDHs are actually capable of reproducing the significant modifications induced by the system on the propagated historical peak flows. This satisfactory result, following those obtained applying the same approach to the routing in a natural lake, in a flood retention reservoir (Tomirotti & Mignosa, 2017) or in seepage problems in river embankments (Butera et al., 2020) suggests that the procedure of derivation of the SDHs is reliable and that the return periods attached to them, at first in a somehow arbitrary way, have some statistical significance. SDHs can then be applied, also together with other approaches, to similar river flood management problems, both in the availability of direct observations and for ungauged sites, due to the possibility of a regional estimation of the SDHs main characteristics.

CRediT authorship contribution statement

Francesca Aureli: Methodology, Supervision, Formal analysis, Investigation, Writing – original draft, Writing – review & editing. **Federico Prost:** Software, Formal analysis, Investigation, Visualization, Writing – review & editing. **Paolo Mignosa:** Supervision, Conceptualization, Methodology, Writing – original draft, Writing – review & editing. **Massimo Tomirotti:** Methodology.

Declaration of Competing Interest

The authors declare that they have no known competing financial interests or personal relationships that could have appeared to influence the work reported in this paper.

Data availability

Maximum averaged discharged QD for the gauging station of interest are available as supplementary data in the attached file

Acknowledgements

The Authors would like to thank the Po River District Basin Authority (AdbPo) for having kindly provided the surveys and DTMs necessary for the preparation of the hydrodynamic model. This research benefited from the HPC (High Performance Computing) facility at the University of Parma, Italy. The Authors gratefully acknowledge also the support of CINECA under the project SCHUBERT: HP10CP2YN9. The positive comments and suggestions of the anonymous Reviewers and of the Editor are gratefully acknowledged.

Appendix A. Supplementary data

Supplementary data to this article can be found online at https://doi.org/10.1016/j.jhydrol.2023.129727.

References

Akaike, H., 1998. Information Theory and an Extension of the Maximum Likelihood Principle. In: Parzen, E., Tanabe, K., Kitagawa, G. (Eds.), Selected Papers of Hirotugu

Akaike. Springer Series in Statistics. Springer, New York, NY. https://doi.org/10.1007/978-1-4612-1694-0_15.
Alfieri, L., Feyen, L., Salamon, P., Thielen, J., Bianchi, A., Dottori, F., Burek, P., 2016. Modelling the socio-economic impact of river floods in Europe. Nat. Hazards Earth Syst. Sci. 16, 1401–1411. https://doi.org/10.5194/nhess-16-1401-2016.
Aricò, C., Nasello, C., Tucciarelli, T., 2009. Using unsteady-state water level data to estimate channel roughness and discharge hydrograph. Adv. Water Resour. 32, 1223–1240. https://doi.org/10.1016/j.advwatres.2009.05.001.
ARPAP-Regional Agency for the Protection of the Environment of Piedmont, https://www.arpa.piemonte.it/rischinaturali/accesso-ai-dati/annali_meteoidrologici/annali-meteo-idro/banca-dati-idrologica.html (accessed on January 14th 2022).
Aureli, F., Prost, F., Vacondio, R., Dazzi, S., Ferrari, A., 2020. A GPU-Accelerated Shallow-Water Scheme for Surface Runoff Simulations. Water 12, 637. https://doi.org/10.3390/w12030637.
Aureli, F., Mignosa, P., Prost, F., Dazzi, S., 2021. Hydrological and Hydraulic Flood Hazard Modeling in Poorly Gauged Catchments: An Analysis in Northern Italy. Hydrology 8, 149. https://doi.org/10.3390/hydrology8040149.
Bacchi, B., Brath, A., Kottegoda, N.T., 1992. Analysis of the Relationships Between Flood Peaks and Flood Volumes Based on Crossing Properties of River Flow Processes. Water Resour. Res. 28 (10), 2773–2782. https://doi.org/10.1029/92WR01135.
Ballarin, C., Maione, U., Mignosa, P. and Tomirotti, M., 2001. Una metodologia di stima indiretta degli idrogrammi sintetici per il progetto di opere di difesa idraulica del territorio, L'Acqua No. 3, 9–16. In Italian. https://www.idrotecnicaitaliana.it/wp-content/uploads/2020/04/Ballarin-et-al-LAcqua-n.-3-2001.pdf.
Barbero, G., Costabile, P., Costanzo, C., Ferraro, D., Petaccia, G., 2022. 2D hydrodynamic approach supporting evaluations of hydrological response in small watersheds: Implications for lag time estimation. J. Hydrol. 610, 127870 https://doi.org/10.1016/j.jhydrol.2022.127870.
Bergmann, H., Sackl, B., 1989. Determination of design flood hydrographs based on regional hydrological data. New directions for surface water modelling. IAHS Publ. no. 181, 261–269.
Brunner, M.I., Seibert, J., Favre, A.C., 2016. Bivariate return periods and their importance for flood peak and volume estimation. Wire's Water 3, 819–833. https://doi.org/10.1002/wat2.1173.
Brunner, M.I., Viviroli, D., Sikorska, A.E., Vannier, O., Favre, A.-C., Seibert, J., 2017. Flood type specific construction of synthetic design hydrographs, Water Resour. Philos. Phenomenol. Res. 53, 1390–1406. https://doi.org/10.1002/2016WR019535.
Brunner, M.I., Sikorska, A.E., Furrer, R., Favre, A.-C., 2018a. Uncertainty assessment of synthetic design hydrographs for gauged and ungauged catchments. Water Resour. Res. 54, 1493–1512. https://doi.org/10.1002/2017WR021129.
Brunner, M.I., Furrer, R., Sikorska, A.E., Viviroli, D., Seibert, J., Favre, A.C., 2018b. Synthetic design hydrographs for ungauged catchments: a comparison of regionalization methods. Stoch. Environ. Res. Risk Assess. 32, 1993–2023. https://doi.org/10.1007/s00477-018-1523-3.
Burnham, K.P., Anderson, D.R., 2002. Model Selection and Multimodel Inference, 2nd ed. Springer, New York.
Butera, I., Climaci, M., Tanda, M.G., 2020. Numerical analysis of phreatic levels in river embankments due to flood events. J. Hydrol. 590, 125382 https://doi.org/10.1016/j.jhydrol.2020.125382.
Buttinger-Kreuzhuber, A., Konev, A., Horváth, Z., Cornel, D., Schwerdorf, I., Blöschl, G., Waser, J., 2022. An integrated GPU-accelerated modeling framework for high-resolution simulations of rural and urban flash floods. Env. Modelling and Software 156, 105480.
Castellarin, A., Kohnova, S., Gaal, L., Fleig, A., Salinas, J.L., Toumazis, A., Kjeldsen, T.R., Macdonald, N., 2012. Review of applied-statistical methods for flood-frequency analysis in Europe, NERC/Centre for Ecology & Hydrology (ESSEM COST Action ES0901).
Catalogo generale dei Beni Culturali, 2014. Resti del Ponte Romano detto "Ponte Vecchio". In Italian. https://catalogo.beniculturali.it/detail/ArchaeologicalProperty/0100354499 (accessed on February 25th 2020).
Chapman, T. G., Maxwell, A.I., 1996. Baseflow Separation - Comparison of Numerical Methods with Tracer Experiments. https://search.informit.org/doi/10.3316/informit.360361071346753.
Chen, L., Singh, V.P., Shenglian, G., Hao, Z., Li, T., 2012. Flood coincidence risk analysis using multivariate copula functions. J. Hydrol. Eng. 17 (6), 742–755. https://doi.org/10.1061/(asce)he.1943-5584.0000504.
Claps, P., Ganora, D., Apostolo, A., Brignolo, I., Monforte, I., 2020. Catalogo delle Piene dei Corsi d'acqua Italiani. CINID, Potenza, Italy. In Italian.
Cook, A., Merwade, V., 2009. Effect of topographic data, geometric configuration and modeling approach on flood inundation mapping. J. Hydrol. 377, 131–142 https://doi.org/10.106110.1016/j.jhydrol.2009.08.015.
Costabile, P., Costanzo, C., De Lorenzo, G., Macchione, F., 2020. Is local flood hazard assessment in urban areas significantly influenced by the physical complexity of the hydrodynamic inundation model? J. Hydrol. 580, 124231 https://doi.org/10.1016/j.jhydrol.2019.124231.
Dazzi S., Vacondio R., Ferrari A., D'Oria M., Mignosa P. 2020b. Flood simulation in urban areas obtained by GPU-accelerated 2D shallow water model with internal boundary conditions. River flow 2020, CRC Press, pp. 1130-1138.
Dazzi, S., Vacondio, R., Mignosa, P., 2019. Integration of a levee breach erosion model in a GPU accelerated 2D shallow water equations code. Water Resour. Res. 55 (1), 682–702. https://doi.org/10.1029/2018WR023826.
Dazzi, S., Vacondio, R., Mignosa, P., 2020a. Internal boundary conditions for a GPU-accelerated 2D shallow water model: Implementation and applications. Adv. Water Resour. 137, 103525 https://doi.org/10.1016/j.advwatres.2020.103525.
Dazzi, S., Shustikova, I., Domeneghetti, A., Castellarin, A., Vacondio, R., 2021. Comparison of two modelling strategies for 2D large-scale flood simulations. Environ. Modelling and Software 146, 105225. https://doi.org/10.1016/j.envsoft.2021.105225.
De Michele, C., Rosso, R., 2001. Uncertainty Assessment of Regionalized Flood Frequency Estimates. J. Hydrol. Eng. 6 (453–702), 459. https://doi.org/10.1061/(ASCE)1084-0699(2001)6:6(453).
De Michele, C., Rosso, R., 2002. A multi-level approach to flood frequency regionalization. Hydrol. Earth Syst. Sci. 6 (2), 185–194. https://doi.org/10.5194/hess-6-185-2002.
Efron, B., Tibshirani, R.J., 1994. An introduction to the Bootstrap. Monographs on Statistics and Applied Probability. Chapman & Hall/CRC.
European Council. EU Flood Directive 2007/60, 2007 (https://eur-lex.europa.eu/legal-content/EN/TXT/?uri=celex:32007L0060).
Fabio, P., Aronica, G.T., Apel, H., 2010. Towards automatic calibration of 2-D flood propagation models. Hydrol. Earth Syst. Sci. 14, 911–924. https://doi.org/10.5194/hess-14-911-2010.
Fabozzi, F.J., Focardi, S.M., Rachev, S.T., Arshanapalli, B.G., 2014. The Basics of Financial Econometrics: Tools, Concepts, and Asset Management Applications. John Wiley & Sons.
Ferrari, A., Dazzi, S., Vacondio, R., Mignosa, P., 2020. Enhancing the resilience to flooding induced by levee breaches in lowland areas: a methodology based on numerical modelling. Natural Hazards and Earth Syst. Sci. 20 (1), 59–72. https://doi.org/10.5194/nhess-20-59-2020.
Ferrari A., D'Oria, M., Vacondio R., Mignosa P., 2022. Automatic calibration of a river reach by coupling a parallel 2D shallow water model and the PEST tool. In Proceedings of the River flow 2022 International Conference; November 8-10 2022; Kingston and Ottawa.
Fischer, S., Schumann, A.H., 2021. Multivariate flood frequency analysis in large river basins considering tributary impacts and flood types. Water Resour. Res. 57 https://doi.org/10.1029/2020WR029029 e2020WR029029.
Franchini, M., Galeati, G., 2000. Comparative analysis of some methods for deriving the expected flood reduction curve in the frequency domain. Hydrol. Earth Syst. Sci. 4 (1), 155–172. https://doi.org/10.5194/hess-4-155-2000.
Ganora, D., Evangelista, G., Cordero, S., Claps, P., 2023. Design flood hydrographs: a regional analysis based on flood reduction functions. Hydrol. Sci. J. 68 (2), 325–340. https://doi.org/10.1080/02626667.2022.2153051.
Goel, N.K., Seth, S.M., Chandra, S., 1998. Multivariate modeling of flood flows. J. Hydraul. Eng. 124 (2), 146–155. https://doi.org/10.1061/(ASCE)0733-9429(1998) 124:2(146).
Gräler, B., van den Berg, M.J., Vandenberghe, S., Petroselli, A., Grimaldi, S., De Baets, B., Verhoest, N.E.C., 2013. Multivariate return periods in hydrology: a critical and practical review focusing on synthetic design hydrograph estimation. Hydrol. Earth Syst. Sci. 17, 1281–1296. https://doi.org/10.5194/hess-17-1281-2013.
Hosking, J.R.M., Wallis, J.R., 1997. Regional Frequency Analysis. Cambridge University Press. ISBN 0521430453.
Huang, K., Chen, L., Zhou, J., Zhang, J., Singh, V.P., 2018. Flood hydrograph coincidence analysis for mainstream and its tributaries. J. Hydrol. 565, 341–353. https://doi.org/10.1016/j.jhydrol.2018.08.007.
Hydrodata, 2002. Studio di fattibilità della sistemazione idraulica del fiume Dora Baltea nel tratto da Aymavilles alla confluenza Po (Feasibility study of the hydraulic restoration of the Dora Baltea river from Aymavilles to the Po confluence). Contract Research Report for AdbPo, In Italian.
Institute of Hydrology, 1999. Flood Estimation Handbook. Institute of Hydrology, UK.
Jiang, W., Yu, J., Wang, Q., Yue, Q., 2022. Understanding the effects of digital elevation model resolution and building treatment for urban flood modelling. J. Hydrol.: Reg. Stud. 42 https://doi.org/10.1016/j.ejrh.2022.101122.
Kao, S.-C., Chang, N.-B., 2012. Copula-based flood frequency analysis at ungauged basin confluences: Nashville. Tennessee. Journal of Hydrol. Eng. 17 (7), 790–799. https://doi.org/10.1061/(ASCE)HE.1943-5584.0000477.
Keifer, C.J., Chu, H.H., 1957. Synthetic storm pattern for drainage design. J. Hydraul. Div. 83, 1–25.
Kendall, M.G., 1975. Rank Correlation Methods, 4th Edition. Charles Griffin, London.
Kottegoda, N.T., Natale, L., Raiteri, E., 2014. Monte Carlo Simulation of rainfall hyetographs for analysis and design. J. Hydrol. 519, 1–11. https://doi.org/10.1016/j.jhydrol.2014.06.041.
Laio, F., Revelli, R., 2003. Uso dei dati storici e sistematici per l'analisi probabilistica delle portate di piena della Dora Baltea. L'Acqua 5, 9–18. In Italian.
Laio, F., Di Baldassarre, G., Montanari, A., 2009. Model selection techniques for the frequency analysis of hydrological extremes. Water Resour. Res. 45, W07416. https://doi.org/10.1029/2007WR006666.
Laio, F., Ganora, D., Claps, P., Galeati, G., 2011. Spatially smooth regional estimation of the flood frequency curve (with uncertainty). J. Hydrol. 408, 67–77. https://doi.org/10.1016/j.jhydrol.2011.07.022.
Liang, Q., Marche, F., 2009. Numerical resolution of well-balanced shallow water equations with complex source terms. Adv. Water Resour. 32, 873–884. https://doi.org/10.1016/j.advwatres.2009.02.010.
Maione, U., Mignosa, P., Tomirotti, M., 2003. Regional estimation of synthetic design hydrographs. Intl. J. River Basin Management 1 (2), 151–163. https://doi.org/10.1080/15715124.2003.9635202.
Mann, H.B., 1945. Nonparametric Tests Against Trend. Econometrica 13 (3), 245. https://doi.org/10.2307/1907187. Accessed on 27 Jan. 2023.
Mediero, L., Jiménez-Álvarez, A., Garrote, L., 2010. Design flood hydrographs from the relationship between flood peak and volume. Hydrol. Earth Syst. Sci. 14, 2495–2505. https://doi.org/10.5194/hess-14-2495-2010.
Mignosa, P., Vacondio, R., Aureli, F., Dazzi, S., Ferrari, A., Prost, F., 2018. High resolution 2D modelling of rapidly varying flows: Some case studies. Ital. J. Eng. Geol. Environ. 143–160 https://doi.org/10.4408/IJEGE.2018-01.S-13.

NERC (National Environmental Research Council), 1975. Flood Studies Report, Vol. 1, London.
Papaioannou, G., Loukas, A., Vasiliades, L., Aronica, G.T., 2016. Flood inundation mapping sensitivity to riverine spatial resolution and modelling approach. Nat. Hazards 83 (Suppl 1), 117–132. https://doi.org/10.1007/s11069-016-2382-1.
Peng, Y., Chen, K., Yan, H., Yu, X., 2017. Improving flood-risk analysis for confluence flooding control downstream using copula Monte Carlo method. J. Hydrol. Eng. 22 (8), 04017018. https://doi.org/10.1061/(asce)he.1943-5584.0001526.
Pettitt, A.N., 1979. A Non-Parametric Approach to the Change-Point Problem. J. R. Soc.: Ser. C (Appl. Stat.) 28, 126–135. https://doi.org/10.2307/2346729.
Requena, A.I., Mediero, L., Garrote, L., 2013. A bivariate return period based on copulas for hydrologic dam design: accounting for reservoir routing in risk estimation. Hydrol. Earth Syst. Sci. 17, 3023–3038. https://doi.org/10.5194/hess-17-3023-2013.
Rosbjerg, D., Blöschl, G., Burn, D.H., Castellarin, A., Croke, B., Di Baldassarre, G., Iacobellis, V., Kjeldsen, T.R., Kuczera, G., Merz, R., Montanari, A., Morris, D., Ouarda, T.B.M.J., Ren, L., Rogger, M., Salinas, J.L., Toth, E., Viglione, A., 2013. Prediction of floods in ungauged basins. In: Blöschl, G., Sivapalan, M., Wagener, T., Viglione, A., Savenije, H. (Eds.), Runoff Prediction in Ungauged Basins: Synthesis across Processes, Places and Scales. Cambridge University Press, pp. 189–226.
Sackl, B., Bergmann, H., 1987. A bivariate flood model and its application. In: Singh, V.P. (Ed.), Hydrologic Frequency Modelling. Reidel, Dordrecht, pp. 571–582.
Salvadori, G., De Michele, C., 2004. Frequency analysis via copulas: theoretical aspects and applications to hydrological events. Water Resour. Res. 40 (12), WR003133. https://doi.org/10.1029/2004WR003133.
Salvadori, G., De Michele, C., Durante, F., 2011. On the return period and design in a multivariate framework. Hydrol. Earth Syst. Sci. 15, 3293–3305. https://doi.org/10.5194/hess-15-3293-2011.
Schubert, J.E., Luke, A., AghaKouchak, A., Sanders, B.F., 2022. A framework for mechanistic flood inundation forecasting at the metropolitan scale. Water Resour. Res. 58 https://doi.org/10.1029/2021WR031279 e2021WR031279.
Schwarz, G., 1978. Estimating the dimension of a model. Ann. Stat. 6, 461–464. https://doi.org/10.1214/aos/1176344136.
Serinaldi, F., Grimaldi, S., 2011. Synthetic design hydrographs based on distribution functions with finite support. J. Hydrol. Eng. 16 (5), 434–446. https://doi.org/10.1061/(ASCE)HE.1943-5584.0000339.
Shiau, J., Wang, H.Y., Tsai, C.T., 2006. Bivariate Frequency Analysis of floods using copulas. J. Am. Water Resour. Assoc. 1549–1564. https://doi.org/10.1111/j.1752-1688.2006.tb06020.x.
Sofia, G., Fontana, G.D., Tarolli, P., 2014. High-resolution topography and anthropogenic feature extraction: Testing geomorphometric parameters in floodplains. Hydrol. Process. 28 (4), 2046–2061. https://doi.org/10.1002/hyp.9727.
Talbot, G., 2023. Extreme values statistical analysis library. https://www.mathworks.com/matlabcentral/fileexchange/93075-extreme-values-statistical-analysis-library, MATLAB Central File Exchange. Retrieved September 1, 2022.
Tomirotti, M., Mignosa, P., 2017. A methodology to derive Synthetic Design Hydrographs for river flood management. J. Hydrol. 555, 736–743. https://doi.org/10.1016/j.jhydrol.2017.10.036.
Toro, E.F., 2001. Shock-Capturing Methods for Free-Surface Shallow Flows. Wiley. ISBN 0471987662.
Vacondio, R., Dal Palù, A., Mignosa, P., 2014. GPU-enhanced finite volume shallow water solver for fast flood simulations. Environ. Modelling & Software 57, 60–75. https://doi.org/10.1016/j.envsoft.2014.02.003.
Vacondio, R., Aureli, F., Ferrari, A., Mignosa, P., Dal Palù, A., 2016. Simulation of the January 2014 flood on the Secchia River using a fast and high-resolution 2D parallel shallow-water numerical scheme. Nat. Hazards 80 (1), 103–125. https://doi.org/10.1007/s11069-015-1959-4.
Vacondio, R., Dal Palù, A., Ferrari, A., Mignosa, P., Aureli, F., Dazzi, S., 2017. A non-uniform efficient grid type for GPU-parallel Shallow Water Equations models. Environ. Modelling & Software 88, 119–137. https://doi.org/10.1016/j.envsoft.2016.11.012.
Vangelis, H., Zotou, I., Kourtis, I.M., Bellos, V., Tsihrintzis, V.A., 2022. Relationship of Rainfall and Flood Return Periods through Hydrologic and Hydraulic Modeling. Water 14, 3618. https://doi.org/10.3390/w14223618.
Viglione, A., Merz, R., Blöschl, G., 2009. On the role of the runoff coefficient in the mapping of rainfall to flood return periods. Hydrol. Earth Syst. Sci. 13, 577–593. https://doi.org/10.5194/hess-13-577-2009.
Wagener, T., Montanari, A., 2011. Convergence of approaches toward reducing uncertainty in predictions in ungauged basins. Water Resour. Res. 47, 6301. https://doi.org/10.1029/2010WR009469.
Wang, C., Chang, N.B., Yeh, G.T., 2009. Copula-based flood frequency (COFF) analysis at the confluences of river systems. Hydrol. Processes: International Journal 23 (10), 1471–1486. https://doi.org/10.1002/hyp.7273.
Westerberg, I.K., Wagener, T., Coxon, G., McMillan, H.K., Castellarin, A., Montanari, A., Freer, J., 2016. Uncertainty in hydrological signatures for gauged and ungauged catchments. Water Resour. Res. 52, 1847–1865. https://doi.org/10.1002/2015WR017635.
Yue, S., 1999. Applying bivariate normal distribution to flood frequency analysis. Water Int. 24 (3), 248–252. https://doi.org/10.1080/02508069908692168.
Yue, S., 2000. The bivariate lognormal distribution to model a multivariate flood episode. Hydrol. Process. 14, 2575–2588. https://onlinelibrary.wiley.com/doi/10.1002/1099-1085(20001015)14:14%3C2575::AID-HYP115%3E3.0.CO;2-L.
Yue, S., 2001a. The Gumbel logistic model for representing a multivariate storm event. Adv. Water Resour. 24, 179–185. https://doi.org/10.1016/S0309-1708(00)00039-7.
Yue, S., 2001b. A bivariate gamma distribution for use in multivariate flood frequency analysis. Hydrol. Process. 15 (6), 1033–1045. https://doi.org/10.1002/hyp.259.
Yue, S., Ouarda, T., Bobée, B., Legendre, P., Bruneau, P., 1999. The Gumbel mixed model for flood frequency analysis. J. Hydrol. 226 (1–2), 88–100. https://doi.org/10.1016/S0022-1694(99)00168-7.
Yue, S., Rasmussen, P., 2002. Bivariate frequency analysis: discussion of some useful concepts in hydrological application. Hydrol. Process. 16, 2881–2898. https://doi.org/10.1002/hyp.1185.
Yue, S., Ouarda, T., Bobée, B., Legendre, P., Bruneau, P., 2002. Approach for describing statistical properties of flood hydrograph. J. Hydrol. Eng. 7 (2), 147–153. https://doi.org/10.1061/(ASCE)1084-0699(2002) 7:2(147).
Zhang, J., 2020. Modern Monte Carlo methods for efficient uncertainty quantification and propagation: A survey. WIREs Comput. Stat. 2021 (13), e1539.
Zhang, Z., Wagener, T., Reed, P., Bhushan, R., 2008. Reducing uncertainty in predictions in ungauged basins by combining hydrologic indices regionalization and multiobjective optimization. Water Resour. Res. 44 https://doi.org/10.1029/2008WR006833.
Zhou, Y., Zhang, D., Zhou, P., Wang, Z., Yang, P., Jin, J., Cui, Y., Ning, S., 2021. Copula-Based Bivariate Return Period Analysis and Its Implication to Hydrological Design Event. JAWRA 1–13. https://doi.org/10.1111/1752-1688.12943.